Proceedings of the Korean Nuclear Society Autumn Meeting
Cheju, Korea, May 2001

Simultaneous Visualization of Bubbles and Dry Spots for Pool Boiling of R-113

H. J. Chung, B. D. Kim, Y. J. Yun, S. Y. Chun, H. C. No*

Korea Atomic Energy Research Institute
PO Box 105 Yusong, Taejon, Korea 305-600

Abstract

A simultaneous visualization of the behavior of bubbles and dry spots has been carried out for pool boiling of R-113 on a horizontal heater. From video imaging and image processing analysis, the formation of bubbles and dry spots occurs simultaneously, and therefore they should be considered as a synchronized concept rather than independent identities. The dry spot density is equivalent to the active site density in the region before CHF. At CHF point, large dry areas due to the coalescence of neighboring dry areas cover the heater surface.

.

1. Introduction

In spite of extensive experimental and theoretical efforts on the Critical Heat Flux (CHF) in pool and flow boiling, there are still considerable disagreements regarding the mechanism of CHF. This may be due to the difficulty in performing detailed visualization of near the wall region at heat fluxes approaching CHF.

The traditional approaches to CHF treat it as a phenomenon independent of the nucleate boiling process immediately preceding it [1], [2], [3]. However, several studies [4], [5] have shown that all parameters affecting nucleate boiling influence the transition boiling region as well. The occurrence of dry areas in the nucleate boiling region near CHF has been observed by several investigators [6], [7], [8]. Thus, it is reasonable and realistic to see that the physical phenomena involved in the nucleate boiling region extend to CHF.

Nucleate boiling is characterized by the presence of bubbles generated from preferential sites randomly located on the heating surface. As a classical photographic study, Gaertner [6] presented the following CHF mechanism. At a higher heat flux mushroom bubbles, which come from coalescence of neighboring vapor columns, coalesce to form large vapor mushrooms separated from the surface by a thin liquid layer.

In Gaertner's experiment, a second transition region was defined where the liquid layer

* Korea Advanced Institute of Science and Technology

partially dried out before the larger mushroom departed. Wide spread vapor patches caused CHF or burnout for his electrically heated system. Based on Gaertner's experimental observation, Haramura and Katto [2] proposed the 'macrolayer dryout model' and Dhir and Liaw [9] proposed the 'unified model' for CHF.

Recently, Nishio et al. [8] presented the outstanding experimental observation results about the liquid-solid contact phenomena. They used a single crystal sapphive as heater material and collected very clear images for the liquid-solid contact phenomena by using the total reflection technique. Nisho et al.'s results showed that the liquid-solid contact pattern was somewhat network like at CHF conditions. These results are very different from Gaertner's representation in which isolated vapor stems with small diameters are attached to the boiling surface.

There are two main reasons for the lack of a complete mechanistic description of CHF. One is the difficulties in direct observation of the physical boiling structure occurring near the boiling surface. The other is that most investigations focus on only one interesting parameter, bubble behavior or dry area formation.

Therefore, in the present study new experimental attempts are made to directly observe the bubble behavior and liquid-solid contact phenomena simultaneously. The synchronized physical images of bubble behavior and the liquid-solid contact phenomena are very helpful to identify the fundamental CHF mechanism.

2. Experimental Method

The experimental facility was made for not only pool boiling but flow boiling. A schematic flow diagram of the experimental facility is shown in Fig. 1. It consists of a test section, condenser, storage tank, Canned motor pump, and preheater. The volumetric flow rate through the test section is measured with a turbine flow meter, and at the outlet of the flow meter a preheater with a heat rate of 20 kW is installed to adjust the inlet fluid temperature. For the pool boiling test, the two valves at the test section inlet and outlet are closed

As shown in Fig. 2, the horizontal visual test section is comprised of 80×80 mm inner dimension mica plates that are 10 mm thick and 0.5 m long. A 10mm thick and 50×50 mm square single crystal sapphire plate is installed at the central part of the bottom plate of the test section. The lower surface of the single crystal sapphire is coated with a transparent electro-conductive film 700 angstroms thick. The boiling surface is heated by supplying a DC electric current to the electro-conductive thin film. In the test section a silicone oil bath is equipped for insulating and refractive index matching. During the pool boiling test four auxiliary heaters,

each of which has a maximum heat capacity of 450 W, are used to maintain the test liquid as saturation temperature.

In the nucleated boiling region, the observation is accomplished under steady state conditions by increasing or decreasing the DC current step by step. The current input to the electro-conductive thin film is controlled with a 250 V, 8A DC power supply. Six K-type thermocouples, four on the lower side and two on the upper side of the sapphire plate, are used to monitor the temperature variation.

As shown in Fig. 2, the laser beam through the beam expander is introduced to the back side of the sapphire plate. When the incident beam is adequately set, the total reflection occurs at the upper surface if the upper surface is dry [10], and it does not occur if the surface is wet by the liquid. In this study, a prism is used to get a wider direct reflection area as shown in Fig. 2. The total reflection images and direct reflection images are then recorded simultaneously to get the synchronized bubble and dry area dynamics.

In this study, as mentioned above, pool boiling of R-113 under the saturation temperature and atmospheric pressure conditions has been carried out from a lower heat flux to a high heat flux (CHF).

3. Experimental Results and Discussion

Photograps were taken from incipience boiling to CHF. High speed video imaging were taken 500 frames/s, and to examine the dynamic behavior of bubbles and dry spots photograps of bubbles and dry spots were taken simultaneously.

3.1 Behavior of Bubbles and Dry Spots

Figure 3 shows a typical set of observed boiling phenomena from incipience boiling to CHF. In Fig. 3, the upper part of each image are bubbles and the lower part dry spots.

Figure 3(a) shows the situation at incipience boiling. There are a few round bubbles and dry spots. When the heat flux increases the number of bubbles and dry spots increases, however their shapes remain round (Fig. 3(b)). The interaction between neighboring bubbles occurs frequently with the increase of heat flux, and results in a coalescence of neighboring dry spots. However, large bubbles and large dry areas are not observed (Figs. 3(c), 3(d)).

Figure 3(e) represents the situation just before CHF. The number of bubbles and dry spots is very high and their size increases further than in the cases of Fig. 3(c). The shapes of the bubbles and dry spots are not round, and this may be due to their active interaction. From figs. 3(a) to 3(c) the liquid-solid contact patterns and wetted patterns show a continuous plane,

whereas the wetted pattern changes into isolated wriggling canals of liquid at the CHF point, as also observed by Oka et al. [11], and Nishio et al. [8]. In Fig. 3(e) tiny vapor stems and large vapor mushrooms are not observed.

3.2 Chronological Behavior of Bubbles and Dry Spots

Figure 4 shows the chronological sequence of bubbles and dry spots at ΔT_{ws} = 23.8 K. The upper part of Fig. 4 represents the bubbles and the lower part represents dry spots. For bubble series A(upper bubbles), bubble A(a) and A(b) are growing, and the dry spots under the corresponding bubbles(upper dry spots) are also growing. Bubble A(c) is in the moment before departing, which results in the decreasing the size of the corresponding dry spot. When the bubble A5 departs, the corresponding dry spot disappears. Similar aspects are shown in the case of growing bubble series B(for lower bubbles and lower dry spots). From this chronological sequence, it can be conclusively noted that bubbles and dry spots occur simultaneously.

3.3 Phenomenological behavior of bubbles and dry spots

The highest heat flux that gave a stable surface temperature was recorded as CHF. Boiling at CHF was observed to occur primarily at the liquid –solid contact region, and the dry areas rather than dry spots fluctuate severely. Figure 6 shows the dynamic behavior of the bubbles and dry spots at CHF. Due to the common recording of detaching bubbles and attached bubbles the bubble dynamics are not clear. However it can be noted that any mushroom bubbles from coalescence of neighboring bubbles are not observed. At heat fluxes slightly greater than CHF the temperature excursion commenced. Once temperature excursion commenced the heater surface is covered with the large vapor film. Also, from the corresponding dry spots tiny vapor stems are not observed also. From the video imaging analysis it can be noted that the large dry areas are formed from the coalescence of neighboring dry areas. This large vapor film forming process is different from the results by Zuber [1] and Haramura and Katto [2].

4. Conclusion

From synchronized high speed video imaging of bubbles and dry spots the following

conclusions can be derived:

1) The formation of bubbles and dry spots occurs simultaneously, and therefore they should be considered as a synchronized concept rather than independent identities.
2) The dry spot density is equivalent to the active site density in the region before CHF.
3) At CHF point, large dry areas due to the coalescence of neighboring dry areas cover the heater surface.

Acknowledgement

This work was supported by financial support for the nuclear R&D program from the Ministry of Science and Technology of Korea.

References

[1] Zuber N., Stability of Boiling Heat Transfer, *ASME Journal of Heat Transfer*, Vol. 80, pp 711-720, 1958.

[2] Haramura Y., and Katto Y., A new hydrodynamic model of critical heat flux, applicable widely to both pool and forced convection boiling on submerged bodies in saturated liquids. *International Journal of Heat and Mass Transfer*, Vol. 26, pp 389-399, 1983.

[3] Kwon Y. M., Chang S. H., A mechanistic critical heat flux model for high-subcooling, high-mass-flux, and small-tube-diameter conditions. Journal of the Korean Nuclear Society, Vol. 32, No. 1, pp 17-33, 2000.

[4] Berenson P. J., Experiments of pool-boiling heat transfer. *International Journal of Heat and Mass Transfer*, Vol. 5, pp 985-999, 1962.

[5] Sadasivan P. et al., Perspective: Issues in CHF modeling-The need for new experiments. *ASME Journal of Heat Transfer*, Vol. 117, pp. 558-567, 1995.

[6] Gaertner R. F., Photographic study of nucleate boiling on a horizontal surface. *ASME Journal of Heat Transfer*, Vol. 87, pp. 17-29, 1965.

[7] Kirby D. B., and Westwater J. W., Bubble and vapor behavior on a heated horizontal plate during pool boiling near burnout. *Chemical Engineering Progress Symposium Series*, Vol. 61, No. 57, pp 238-248, 1965.

[8] Nishio S. et al., Observation of boiling structures in high heat- flux boiling. *International Journal of Heat and Mass Transfer*, Vol. 41, pp 3191-3201, 1998.

[9] Liaw S. P., and Dhir V. K., Void fraction measurements during saturated pool boiling of

water on partially wetted vertical surfaces. *ASME Journal of heat Transfer*, Vol. 111, pp 731-738, 1989.

[10] Gasvik K. J., *Optical Metrology*. Second edition, John Wiley and Sons, 1996

[11] Oka T. et al., A pool boiling of n-pentane, CFC-113, and water under reduced gravity: Parabolic flight experiments with a transparent heater. *ASME Journal of Heat Transfer*, Vol. 117, pp 406-417, 1995.

[12] Ramanujapu N., and Dhir V. K., Dynamics of contact angle during growth and detachment of a vapor bubble at a single nucleation site. *Proceedings of the 5th ASME/JSME Joint Thermal Engineering Conference*, San Diego, U.S.A., ASTE99/6277, pp 1-7, 1999.

[13] Afify M. A., and Fruman D. H., Visualization of nucleate pool boiling of Freon 113. *Proceedings of the 4th International Symposium on Flow Visualization*, Paris, France, pp 571-576, 1986.

[14] Kocamustafaogullari G., Ishii M., Interfacial area and nucleation site density in boiling systems. *International Journal of Heat and Mass Transfer*, Vol. 26, No. 9, pp 1377-1387, 1983.

[15] Wang C. H., Dhir V. K., Effect of surface wettability on active nucleation site density during pool boiling of water on a vertical surface. *ASME Journal of Heat Transfer*, Vol. 115, pp 659-669, 1993.

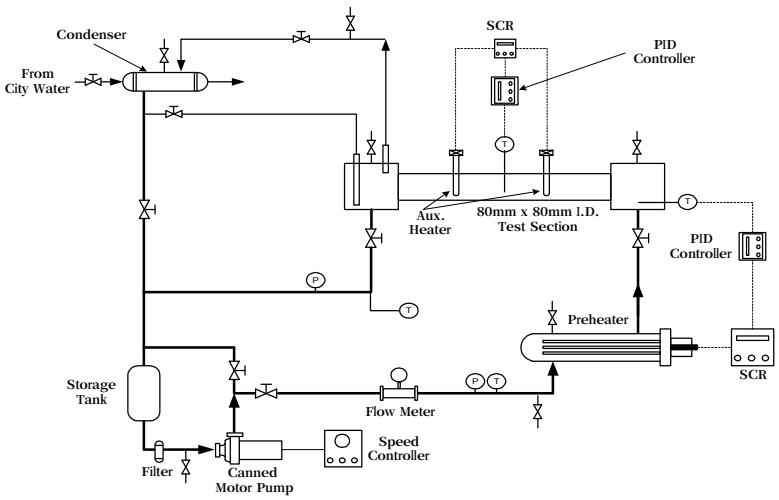

Fig. 1 Schematic flow diagram of the test loop

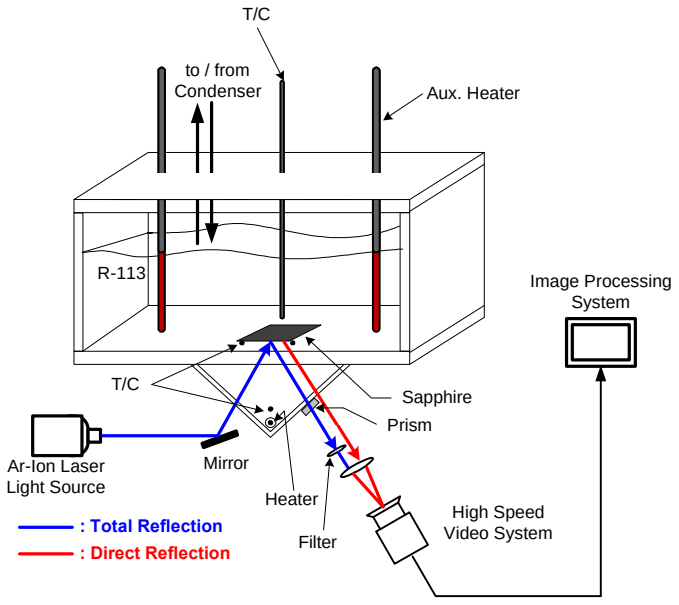

Fig. 2 Horizontal test section

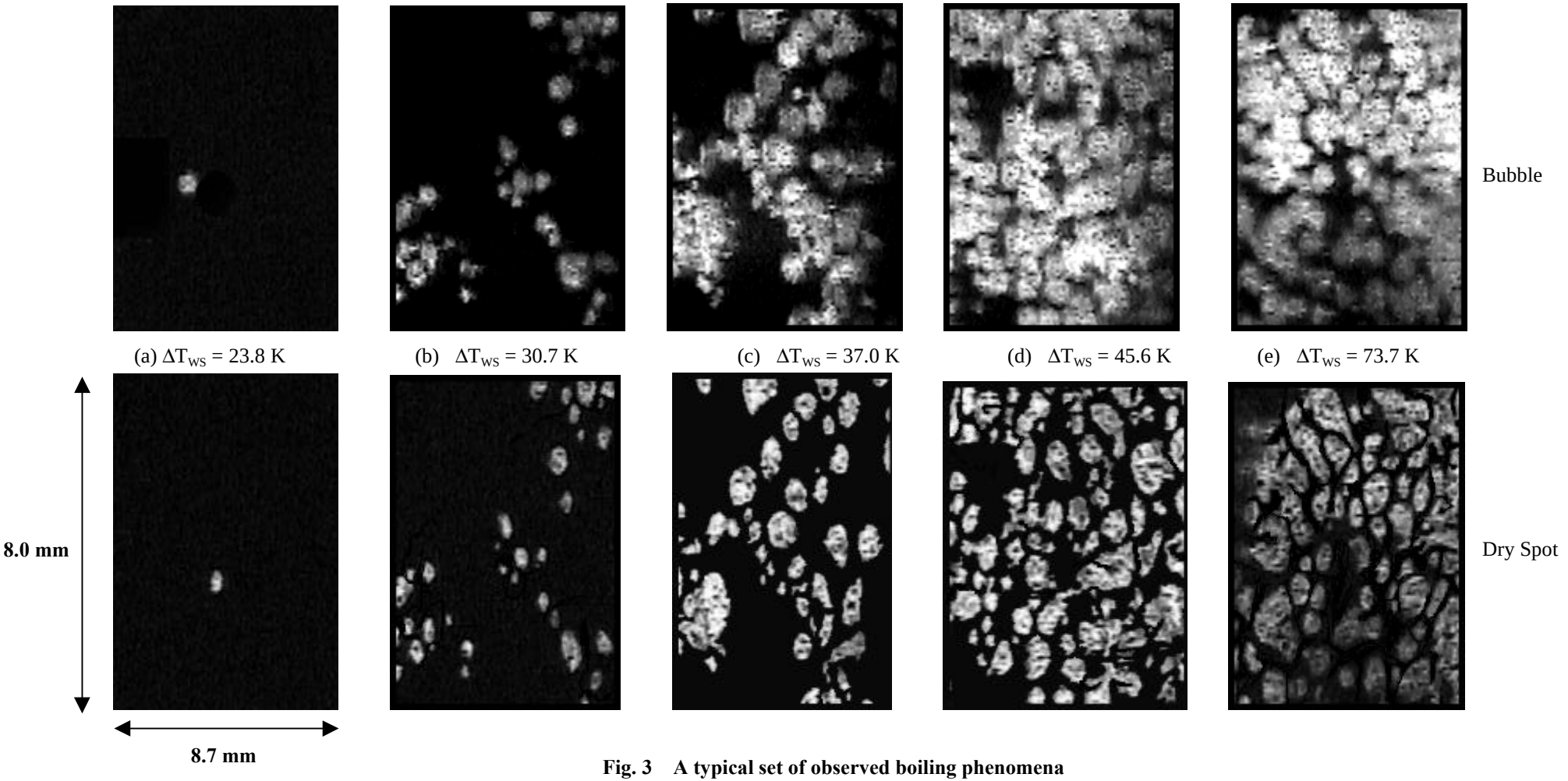

Fig. 3 A typical set of observed boiling phenomena

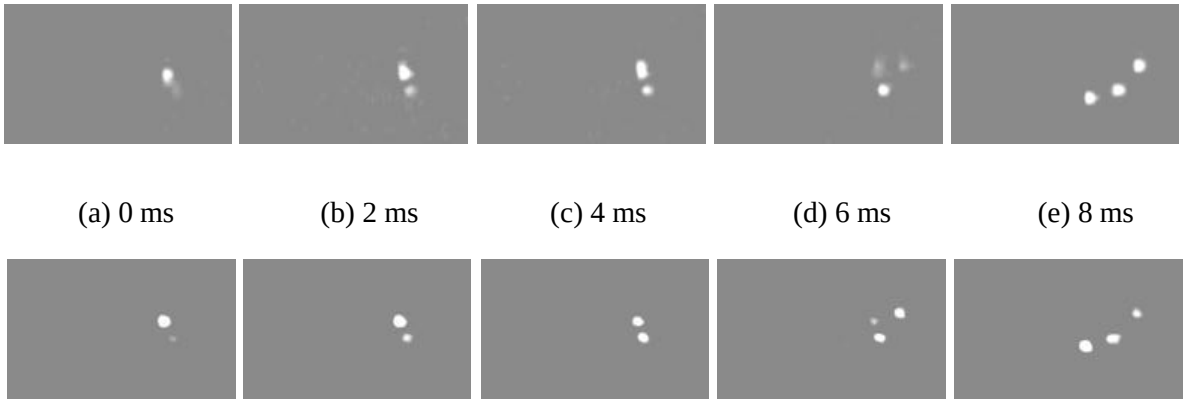

(a) 0 ms (b) 2 ms (c) 4 ms (d) 6 ms (e) 8 ms

Fig. 4. Chronological sequence of bubbles and dry spots at a low heat flux

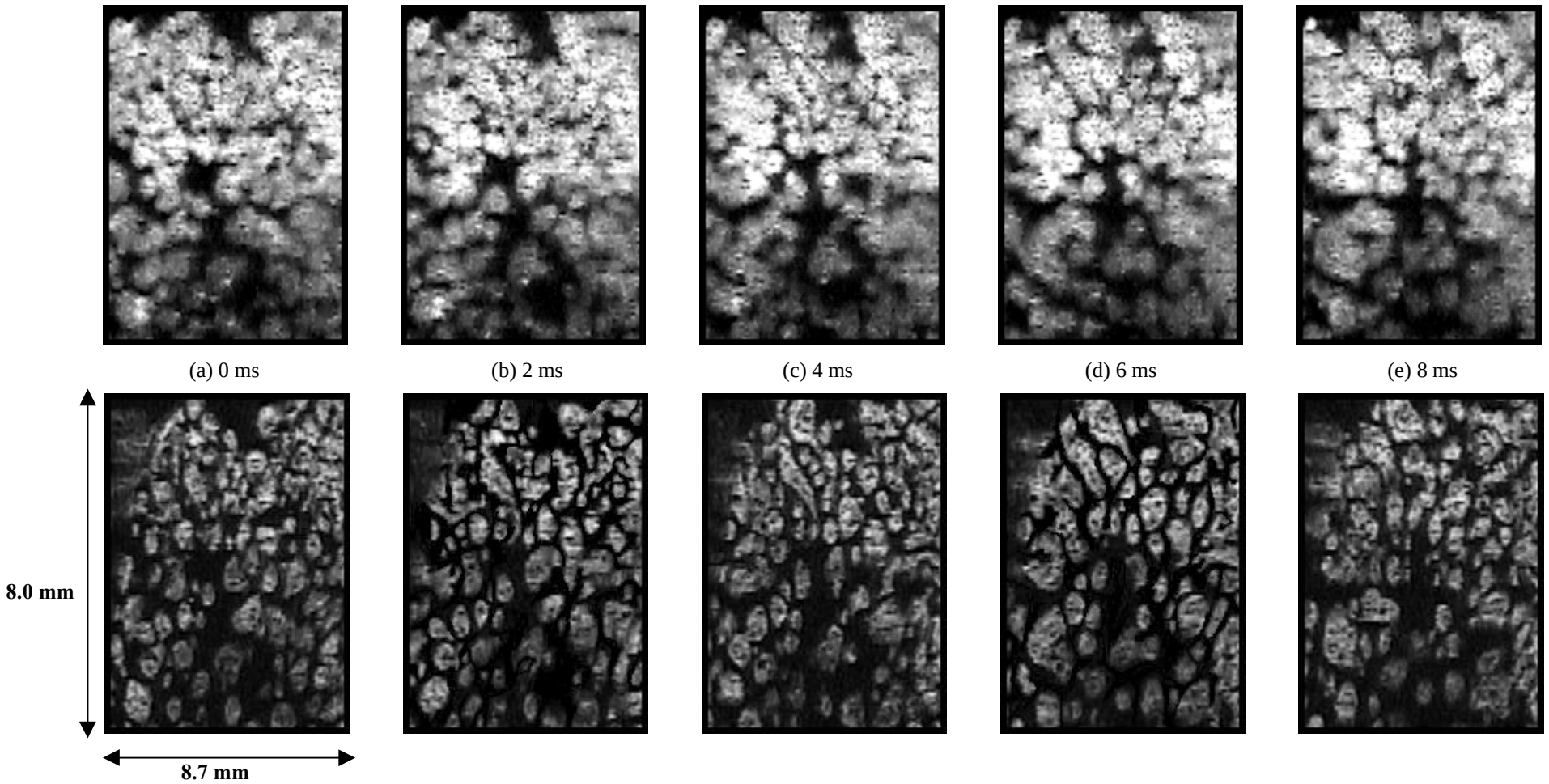

Fig. 5 A typical set of observed boiling phenomena at CHF